Journal of Alloys and Compounds 509 (2011) 7559–7564

Contents lists available at ScienceDirect

Journal of Alloys and Compounds

journal homepage: www.elsevier.com/locate/jallcom

Peculiarity of component interaction in {Y, Dy}–Mn–Sn ternary systems

V.V. Romaka[a], M. Konyk[b], L. Romaka[b,*], V. Pavlyuk[b,c], H. Ehrenberg[d], A. Tkachuk[b]

[a] Department of Materials Engineering and Applied Physics, Lviv Polytechnic National University, Ustyyanovycha Str. 5, 79013 Lviv, Ukraine
[b] Inorganic Chemistry Department, Ivan Franko Lviv National University, Kyryla and Mefodiya Str. 6, 79005 Lviv, Ukraine
[c] Jan Dlugosz University, Institute of Chemistry, Environmental Protection and Biotechnology, al. Armii Krajowej 13/15, 42200 Czestochowa, Poland
[d] Institute for Complex Materials, IFW Dresden, Helmholtzstrasse 20, D-01069 Dresden, Germany

ARTICLE INFO

Article history:
Received 17 January 2011
Received in revised form 19 April 2011
Accepted 20 April 2011
Available online 27 April 2011

Keywords:
Stannides
Phase diagrams
Crystal structure
X-ray diffraction
EPMA

ABSTRACT

The phase equilibria in the Y–Mn–Sn and Dy–Mn–Sn ternary systems were studied at 770 K by means of X-ray and metallographic analyses in the whole concentration range. Both Y–Mn–Sn and Dy–Mn–Sn systems are characterized by formation of two ternary compounds RMn_6Sn_6 ($MgFe_6Ge_6$-type, space group $P6/mmm$) and $R_4Mn_4Sn_7$ ($Zr_4Co_4Ge_7$-type, space group $I4/mmm$). The disorder in $Dy_4Mn_4Sn_7$ compound was found by single crystal method. Compounds with the same type of structure were also found with Gd, Tb, Ho, Er, Tm (confirmed), Yb, and Lu and their lattice parameters were determined.

1. Introduction

The Mn-containing ternary systems with rare earth metals (R) and tin are not yet completely studied. The R–Mn–Sn ternary phase equilibrium diagrams have already been established for Ce and Nd [1,2]. A maximum of four compounds was found in the case of R = Nd at 1073 K, $Nd_5(Mn,Sn)_3$, $Nd_3Mn_4Sn_4$, Nd_5MnSn_5, and $NdMn_{1-x}Sn_{2-y}$ (two ternary compounds $NdMn_{1-x}Sn_{2-y}$ and $NdMn_6Sn_6$ at 818 K), whereas three compounds ($Ce_3Mn_4Sn_4$, $CeMn_{1-x}Sn_{2-y}$, $Ce_2Mn_5Sn_3$) were observed in the Ce–Mn–Sn system. Other systems were studied only to identify isostructural series of compounds for crystallographic parameters and physical property investigations. For R–Mn–Sn systems, where R are heavy rare earth elements, previously the existence one series of the ternary phases only, RMn_6Sn_6, crystallizing with hexagonal $MgFe_6Ge_6$-type, closely related to the $CaCu_5$- and $ThMn_{12}$-type structure, was found [3,4]. Later, the crystal structures were studied by single crystal method for the new ternary stannides with manganese, $Tm_4Mn_4Sn_7$ ($Zr_4Co_4Ge_7$-type) [5], $Yb_4Mn_2Sn_5$ (Mg_5Si_6-type) [6], and R_3MnSn_{5-x} ($Hf_3Cr_2Si_4$-type, R = Tm, Lu) [7].

In this paper we present for the first time the results of X-ray and EPMA analyses of the phase equilibria in the Y–Mn–Sn and Dy–Mn–Sn ternary systems at 770 K and the crystal structure data for the ternary compounds.

2. Experimental

The samples were prepared by arc melting the constituent elements (Dy, purity 99.9 wt.%, Y 99.9 wt.%, Mn 99.98 wt.%, and Sn 99.999 wt.%) under purified, Ti-gettered, argon atmosphere with non-consumable tungsten electrode on a water-cooled copper hearth. The overall weight losses were generally less than 1 wt.%. The alloys were annealed at 770 K for 720 h in an evacuated quartz ampoules, and finally quenched in cold water.

Phase analysis was performed using X-ray powder diffractions of the synthesized samples (DRON-2.0M, Fe $K\alpha$ radiation). The observed diffraction intensities were compared with reference powder patterns of binary and known ternary phases. The compositions of the obtained samples were examined by Scanning Electron Microscopy (SEM) using REMMA-102-02 scanning microscope. Quantitative electron probe microanalysis (EPMA) of the phases was carried out by using an energy-dispersive X-ray analyzer with the pure elements as standards (an acceleration voltage was 20 kV; *K*- and *L*-lines were used). The data for the crystal structure refinements were collected at room temperature using STOE STADI P diffractometer (linear PSD detector, $2\theta/\omega$-scan; Cu $K\alpha_1$ radiation, curved germanium (1 1 1) monochromator). Calculations of the unit cell parameters and theoretical patterns were performed using the CSD [8] and PowderCell [9] program packages. Rietveld refinement of crystal structure was performed using WinPLOTR program package [10].

For the single crystal investigation intensity data were obtained on Enraf-Nonius CAD-4 diffractometer and Bruker Kappa APEXII CCD area-detector diffractometer, graphite-monochromated Mo K_α radiation. Calculations were carried out using SHELXTL package [11].

3. Results and discussion

3.1. Phase equilibria

The phase equilibria in the Y–Mn–Sn and Dy–Mn–Sn phase diagrams have been investigated at 770 K using the X-ray and

* Corresponding author.
E-mail addresses: romakal@franko.lviv.ua, romakav@yahoo.com (L. Romaka).

0925-8388/$ – see front matter © 2011 Elsevier B.V. All rights reserved.
doi:10.1016/j.jallcom.2011.04.110

Table 1
Crystallographic characteristics of the ternary compounds in the {Y, Dy}–Mn–Sn system.

No.[a]	Compound	Space group	Structure type	Lattice parameters, nm		
				a	*b*	*c*
1	$Y_4Mn_4Sn_7$	*I*4/*mmm*	$Zr_4Co_4Ge_7$	1.5104(2)	–	0.5888(1)
2	YMn_6Sn_6	*P*6/*mmm*	$MgFe_6Ge_6$	0.55280(7)	–	0.89966(12)
1	$Dy_4Mn_4Sn_7$	*I*4/*mmm*	$Zr_4Co_4Ge_7$	1.49942(10)	–	0.58991(4)
2	$DyMn_6Sn_6$	*P*6/*mmm*	$MgFe_6Ge_6$	0.55308(1)	–	0.90265(4)

[a] The compounds number corresponds to the figures in the phase diagram (Figs. 1 and 2).

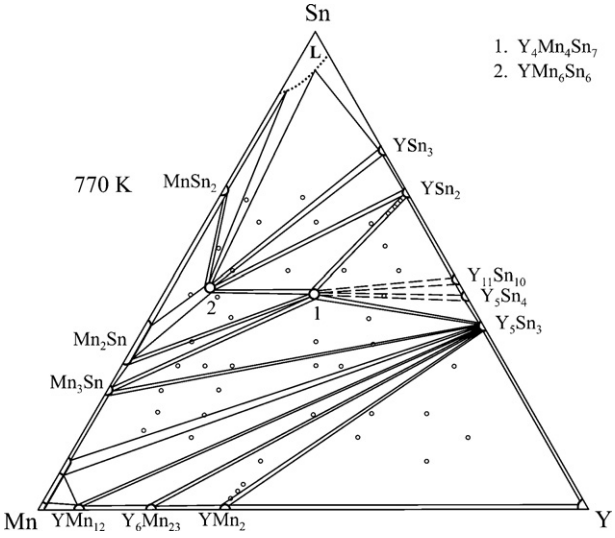

Fig. 1. Isothermal section of the Y–Mn–Sn system at 770 K.

metallographic analyses of 10 binary and 57 ternary alloys for Y system and 11 binary and 69 ternary alloys for Dy system. The isothermal sections of the Y–Mn–Sn and Dy–Mn–Sn ternary systems at corresponding temperatures are presented in Figs. 1 and 2, respectively. The SEM pictures and phases compositions of some alloys are shown in Fig. 3. The compositions and the crystallographic parameters of the formed compounds are listed in Table 1.

The presence of almost all binary compounds in the {Y, Dy}–Mn (RMn_2, R_6Mn_{23}, RMn_{12}), Mn–Sn (Mn_3Sn, Mn_2Sn, $MnSn_2$) and {Y, Dy}–Sn systems (RSn_3, Dy_3Sn_7, RSn_2, $R_{11}Sn_{10}$, R_5Sn_4, R_5Sn_3) [12,13] corresponding to the reference data was confirmed. Due to a high chemical activity of the alloys in the composition range from

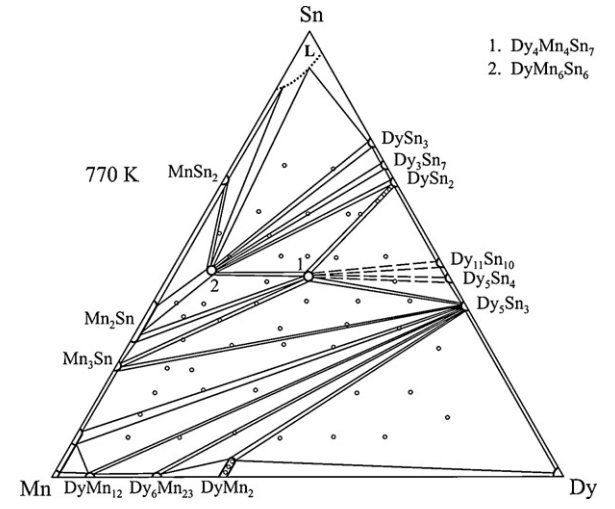

Fig. 2. Isothermal section of the Dy–Mn–Sn system at 770 K.

40 to 65 at.% Sn content, diffraction peaks, which correspond to the theoretical powder patterns of R_5Sn_4 and $R_{11}Sn_{10}$, were observed only on the powder patterns of some ternary alloys in the region close to the stoichiometric composition of these compounds. The formation of the $DyMn_{2-x}Sn_x$ solid solution formed by substitution of the manganese atoms by tin in $DyMn_2$ ($MgCu_2$-type) up to 2 at.% Sn was found. The compositions and values of the lattice parameters are given in Table 2. No solid solution range for the YMn_2 binary compound in the Y–Mn–Sn system was observed. To check the formation of the interstitial solid solution based on the YSn_2 and $DySn_2$ ($ZrSi_2$-type) binary compounds [14,15] the several alloys up to composition $R_{30}Mn_{10}Sn_{60}$ were prepared. Phase analysis of the corresponding samples and the systematic analysis of the cell parameters did not indicated a solubility of Mn in the YSn_2 and $DySn_2$ compounds at investigated temperature.

3.2. Crystal structure

Phase relations in both, Y–Mn–Sn and Dy–Mn–Sn systems are characterized by the formation of two ternary stannides at 770 K, i.e. RMn_6Sn_6 and $R_4Mn_4Sn_7$. The detailed description and analysis of the crystal structure of the $DyMn_6Sn_6$ compound was published in our previous manuscript [16]. Single crystals of YMn_6Sn_6 used for structure refinements were isolated from the crushed ingots of the annealed $Y_8Mn_{46}Sn_{46}$ sample. Crystal structure calculations confirmed a hexagonal $MgFe_6Ge_6$-type (space group *P*6/*mmm*) [17]. The experimental details of single crystal X-ray analysis of the YMn_6Sn_6 compound are listed in Table 3. The refined crystallographic parameters are collected in Tables 4 and 5.

The powder pattern reflections of the $Dy_{26}Mn_{26}Sn_{48}$ sample were indexed on the basis of a tetragonal lattice. Further analysis of the *hkl* reflections and their intensities showed that structure belongs to the $Zr_4Co_4Ge_7$-type (space group *I*4/*mmm*). The crystal structure refinement was performed by single crystal method. At first the structure was refined with fully occupied atomic positions according to the $Zr_4Co_4Ge_7$-type. However the difference Fourier map contained additional maxima, which were not described by the initial model. The model was improved and refined with vacancies in site Sn_4 (8*i*) and additional partially occupied site Sn_5 (4*c*). Thus the refinement results for both ordered and disordered models are presented in Table 3. The final atomic and displacement parameters for ordered model are listed in Tables 6 and 7, and for disordered model in Tables 8 and 9, respectively. Both crystal structure models of the $Dy_4Mn_4Sn_7$ compound are shown in Fig. 4. It should be noted that practically the same disorder was observed

Table 2
Composition and lattice parameters of the samples of the $DyMn_{2-x}Sn_x$ solid solution.

Composition	Lattice parameter, nm *a*	*V*, nm^3
$Dy_{33}Mn_{67}$	0.75924(2)	0.4376(1)
$Dy_{33}Ni_{65}Sn_2$	0.76135(8)	0.4413(2)
[a]$Dy_{33}Mn_{64}Sn_3$	0.76132(8)	0.4412(7)

[a] Two phase sample.

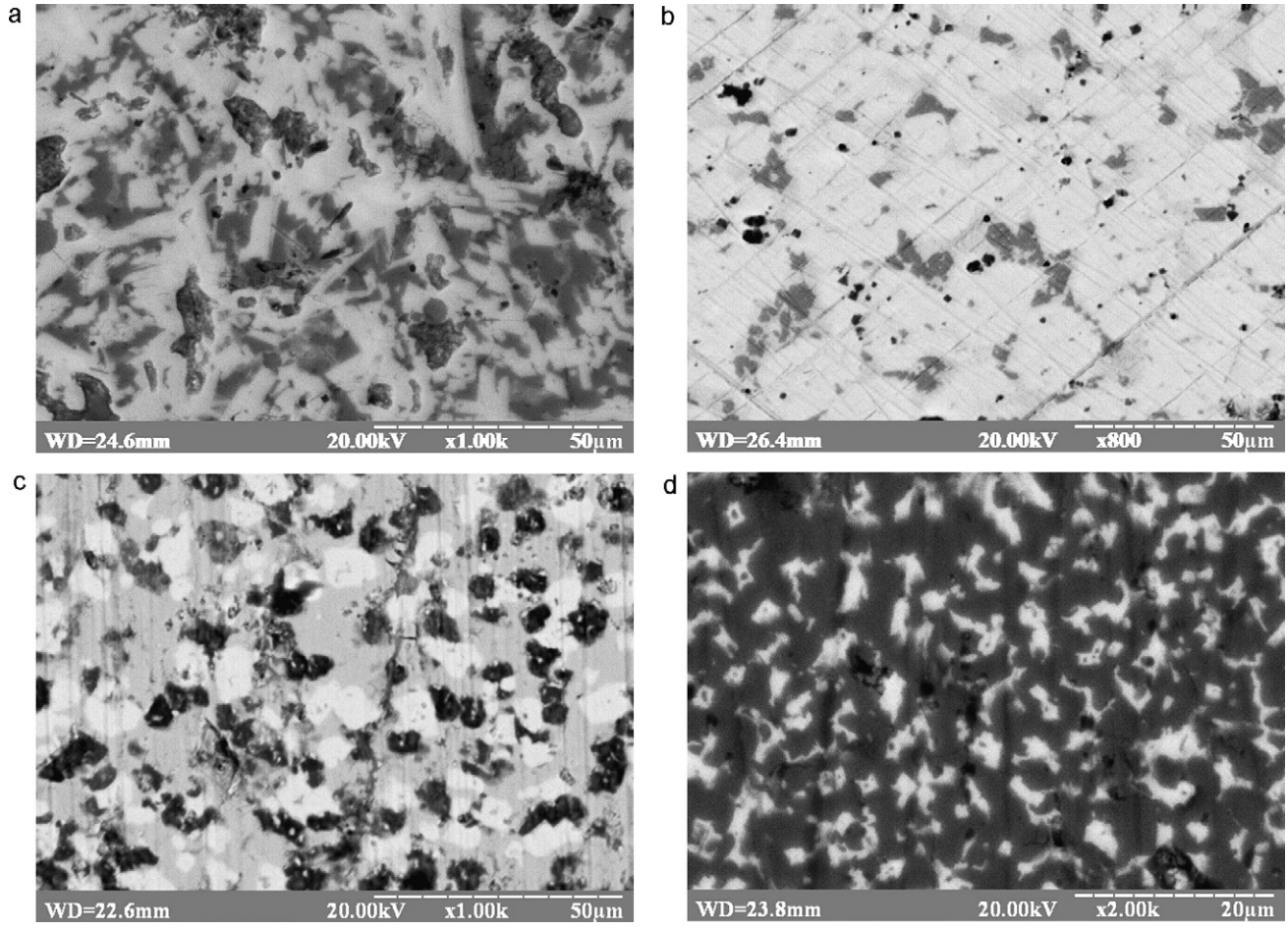

Fig. 3. Electron microphotographs of the alloys: (a) $Y_{31}Mn_{36}Sn_{33}$–$Y_4Mn_4Sn_7$ (grey phase); Y_5Sn_3 (grey light phase); Mn_3Sn (grey dark phase); (b) $Y_{15}Mn_{45}Sn_{40}$–$Y_4Mn_4Sn_7$ (grey light phase), YMn_6Sn_6 (grey phase); Mn_2Sn (grey dark phase); (c) $Dy_7Mn_{56}Sn_{37}$–$Dy_4Mn_4Sn_7$ (grey phase); Mn_2Sn (grey dark phase); $DyMn_6Sn_6$ (grey light phase); (d) $Dy_{10}Mn_{58}Sn_{32}$–$Dy_4Mn_4Sn_7$ (grey phase), Mn_3Sn (grey dark phase).

Table 3
Crystallographic data and experimental details for YMn_6Sn_6 and $Dy_4Mn_4Sn_7/(Dy_4Mn_4Sn_{6.78})$[a] compounds.

Formula	YMn_6Sn_6	$Dy_4Mn_4Sn_7/(Dy_4Mn_4Sn_{6.78})$[a]
Formula mass (amu)	1130.7	1700.6/(1673.9)[a]
Space group	*P*6/*mmm* (191)	*I*4/*mmm* (139)
a (nm)	0.55280(7)	1.49942(10)
b (nm)	0.55280(7)	1.49942(10)
c (nm)	0.89966(12)	0.58991(4)
V (nm^3)	0.23809(1)	1.32627(15)
Z	1	4
Crystal dimensions (mm)	$0.12 \times 0.04 \times 0.04$	$0.09 \times 0.12 \times 0.14$
Diffractometer	Bruker Kappa APEXII CCD area-detector	Enraf-Nonius CAD-4
D_x ($mg\,m^{-3}$)	7.887	8.517/(8.383)[a]
Radiation (Mo *K*α)	(λ = 0.071073 nm)	(λ = 0.071073 nm)
Monochromator	Graphite	Graphite
μ (Mo *K*α) (mm^{-1})	29.01	38.74/(38.33)[a]
θ_{min}, θ_{max} (°)	2.26, 30.32	1.92, 30.50
No. of data collected	2651 (R_{int} = 0.046)	7834 (R_{int} = 0.047)
Reflections with $I > 2\sigma(I)$	186	600
$\Delta\rho_{max}$, $\Delta\rho_{min}$ ($e \times nm^{-3}$) × 10^3	0.287, −0.927	12.665, −5.596/(1.632, −1.534)[a]
$R[F^2 > 2\sigma(F^2)]$	0.022	0.035/(0.024)[a]
$wR(F^2)$	0.070	0.091/(0.055)[a]
S	0.865	1.107/(1.439)[a]
Extinction coefficient	0.023(2)	0.00032(4)/(0.00034(3))[a]
No. of parameters	16	30/(32)[a]

[a] In parentheses the data for disordered model is given.

Table 4
Atomic and thermal parameters for YMn_6Sn_6 compound.

Atom	Wyckoff position	*x*/*a*	*y*/*b*	*z*/*c*	$U_{eq}/B_{iso} \times 10^2$ (nm^2)
Y	1*a*	0	0	1/2	0.0079(4)
Mn	6*i*	1/2	0	0.25288(7)	0.0049(3)
Sn1	2*e*	0	0	0.16246(7)	0.0063(3)
Sn2	2*c*	1/3	2/3	1/2	0.0052(3)
Sn3	2*d*	1/3	2/3	0	0.0062(3)

Table 5
Anisotropic atomic displacement parameters (10^2 nm^2) of YMn_6Sn_6.

Atom	U_{11}	U_{22}	U_{33}	U_{12}	U_{13}	U_{23}
Y	0.0073(5)	0.0073(5)	0.0091(7)	0.0036(2)	0	0
Mn	0.0029(6)	0.0042(5)	0.0071(5)	0.0015(3)	0	0
Sn1	0.0054(3)	0.0054(3)	0.0081(5)	0.0027(2)	0	0
Sn2	0.0046(3)	0.0046(3)	0.0066(4)	0.0023(2)	0	0
Sn3	0.0060(4)	0.0060(4)	0.0064(4)	0.0030(2)	0	0

Table 6
Atomic coordinates and equivalent displacement parameters (10^2 nm^2) of ordered $Dy_4Mn_4Sn_7$.

Atom	Site	*x*/*a*	*y*/*b*	*z*/*c*	U_{eq}
Dy1	8*i*	0.19550(6)	0	0	0.0106(2)
Dy2	8*h*	0.36084(4)	*x*	0	0.0098(2)
Mn	16*k*	0.14975(10)	0.64975(10)	1/4	0.0132(4)
Sn1	8*j*	0.21148(9)	1/2	0	0.0123(3)
Sn2	8*h*	0.20348(6)	*x*	0	0.0101(3)
Sn3	4*e*	0	0	0.2504(3)	0.0100(3)
Sn4	8*i*	0.40604(12)	0	0	0.0267(4)

Table 7
Anisotropic atomic displacement parameters (10^2 nm^2) of ordered $Dy_4Mn_4Sn_7$.

Atom	U_{11}	U_{22}	U_{33}	U_{12}	U_{13}	U_{23}
Dy1	0.0136(4)	0.0090(4)	0.0090(4)	0.000	0	0
Dy2	0.0104(3)	0.0104(3)	0.0086(4)	0.0002(3)	0	0
Mn1	0.0136(6)	0.0136(6)	0.0124(9)	0.0003(7)	0.0005(6)	−0.0005(6)
Sn1	0.0140(6)	0.0099(5)	0.0130(6)	0	0	0
Sn2	0.0096(4)	0.0096(4)	0.0110(6)	−0.0002(4)	0	0
Sn3	0.0112(5)	0.0112(5)	0.0076(7)	0	0	0
Sn4	0.0230(8)	0.0208(8)	0.0363(9)	0	0	0

Table 8
Atomic coordinates and equivalent displacement parameters (10^2 nm^2) of disordered $Dy_4Mn_4Sn_7$.

Atom	Site	*x*/*a*	*y*/*b*	*z*/*c*	U_{eq}
Dy1	8*i*	0.19555(3)	0	0	0.01124(14)
Dy2	8*h*	0.36079(2)	*x*	0	0.01033(13)
Mn	16*k*	0.14974(5)	0.64974(5)	1/4	0.0135(2)
Sn1	8*j*	0.21146(5)	1/2	0	0.01289(16)
Sn2	8*h*	0.20351(3)	*x*	0	0.01066(16)
Sn3	4*e*	0	0	0.25038(17)	0.01060(19)
Sn4[a]	8*i*	0.40603(6)	0	0	0.0198(3)
Sn5[b]	4*c*	1/2	0	0	0.0198(3)

[a] SOF = 0.853(4).
[b] SOF = 0.075(4).

Table 9
Anisotropic atomic displacement parameters (10^2 nm^2) of disordered $Dy_4Mn_4Sn_7$.

Atom	U_{11}	U_{22}	U_{33}	U_{12}	U_{13}	U_{23}
Dy1	0.0142(2)	0.0097(2)	0.0097(2)	0	0	0
Dy2	0.01100(16)	0.01100(16)	0.0090(2)	0.00021(15)	0	0
Mn1	0.0141(3)	0.0141(3)	0.0124(5)	0.0001(4)	0.0005(3)	−0.0005(3)
Sn1	0.0145(3)	0.0105(3)	0.0137(3)	0	0	0
Sn2	0.0102(2)	0.0102(2)	0.0117(3)	−0.0002(2)	0	0
Sn3	0.0119(3)	0.0119(3)	0.0080(4)	0	0	0
Sn4	0.0159(5)	0.0148(5)	0.0287(5)	0	0	0
Sn5	0.0159(5)	0.0148(5)	0.0287(5)	0	0	0

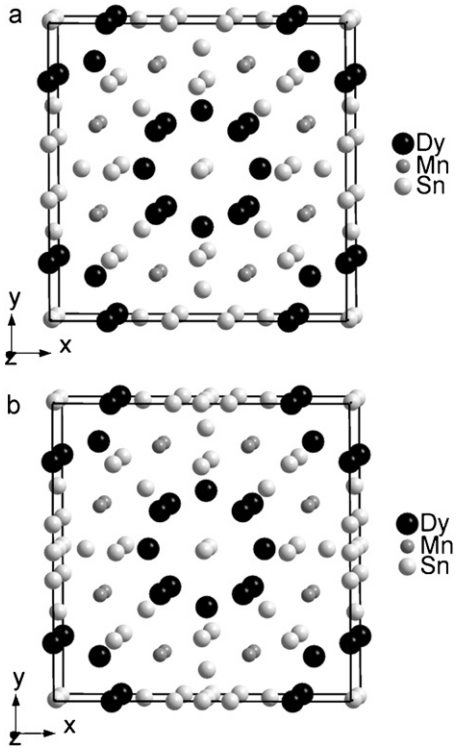

Fig. 4. Model of the $Dy_4Mn_4Sn_7$ structure: (a) ordered ($Dy_4Mn_4Sn_7$) and (b) disordered ($Dy_4Mn_4Sn_{6.78}$).

for 2 additional single crystals (one was grown from the melt, the other one was selected from as-cast sample).

The analysis of the interatomic distances in $Dy_4Mn_4Sn_7$ structures showed that the distance Sn_4–Sn_4 (0.2818 nm) is shorter than the sum of the respective atomic radii (r_a(Sn) = 0.158 nm), but it is almost equal to the sum of their covalent radii (r_c(Sn) = 0.141 nm). The $Dy_4Mn_4Sn_7$ stannide contains similar structural fragments (deformed octahedrons) as other ternary and binary intermetallics – $Dy_{11}Sn_{10}$ [18] and $Dy_{117}Co_{57}Sn_{112}$ [19] (Fig. 5). Thus, crystal chemical analysis showed that $Dy_4Mn_4Sn_7$, $DyMn_6Sn_6$, and YMn_6Sn_6 intermetallic compounds are characterized by the presence of metallic and ion-covalent bonds, caused by the high content of Sn. Stannides $R_4Mn_4Sn_7$, with $Zr_4Co_4Ge_7$-type structure were also found with Gd, Tb, Ho, Er, Tm (confirmed), Yb, and Lu and their lattice parameters are listed in Table 10. One can see that unit cell volume gradually decrease from Y to Lu. The exception is $Yb_4Mn_4Sn_7$ compound, where unit cell volume does not fit the general tendency and could be explained by the presence of Yb^{2+} ion.

Previous investigations performed mostly with light but large rare-earth atoms (Ce, Nd) have shown that the R–Mn–Sn ternary systems contain a relatively small number of ternary phases, for a maximum of four. Furthermore, investigated systems {Y, Dy}–Mn–Sn with heavier but smaller rare-earth atoms have revealed the existence two ternary phases only. Nevertheless, a similarity in RMn_6Sn_6 stoichiometry was observed for light (R = Pr, Nd, Sm) [20] rare-earths. The *f*-element contribution to the chemical and structural characteristics of ternary phases generates different structure types for RMn_6Sn_6 compounds passing from light rare-earths ($HoFe_6Sn_6$-type, built upon an intergrowth of $MgFe_6Ge_6$- and $ScFe_6Ga_6$-blocks) [20,21] to heavy rare-earth elements with fully ordered $MgFe_6Ge_6$-type [3,22], while for $SmMn_6Sn_6$ compound two structural modifications ($MgFe_6Ge_6$- and YCo_6Ge_6-types) were observed depending of the annealing temperature [3,23].

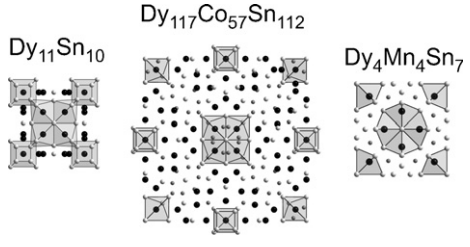

Fig. 5. Similarities of $Dy_4Mn_4Sn_7$ stannide with structures of some related compounds.

Table 10
Lattice parameters of isostructural $R_4Mn_4Sn_7$ compounds.

Compound	Lattice parameters		V, nm^3
	a	c	
$Y_4Mn_4Sn_7$	1.5104(2)	0.5888(1)	1.3432(3)
$Gd_4Mn_4Sn_7$	1.5247(3)	0.5901(1)	1.3718(5)
$Tb_4Mn_4Sn_7$	1.5049(2)	0.5909(1)	1.3382(3)
$Dy_4Mn_4Sn_7$	1.4991(2)	0.5898(1)	1.3255(3)
$Ho_4Mn_4Sn_7$	1.4917(3)	0.5982(1)	1.3311(4)
$Er_4Mn_4Sn_7$	1.4869(3)	0.5951(1)	1.3157(4)
$Tm_4Mn_4Sn_7$	1.4735(3)	0.6055(1)	1.3147(4)
$Yb_4Mn_4Sn_7$	1.5782(3)	0.5901(2)	1.4698(6)
$Lu_4Mn_4Sn_7$	1.4673(3)	0.6021(2)	1.2963(6)

4. Conclusions

The isothermal sections of the {Y, Dy}–Mn–Sn ternary systems were constructed at 770 K and are characterized by formation of stannides with general formula RMn_6Sn_6 and $R_4Mn_4Sn_7$. The crystal structure analysis showed that $Dy_4Mn_4Sn_7$ is disordered. Isostructural $R_4Mn_4Sn_7$ compounds were also found with Gd, Tb, Ho, Er, Tm, Yb, and Lu. All investigated stannides are characterized by the presence of metallic and ion-covalent bonding due to high Sn content in the structures.

Acknowledgement

The work was supported by the Ministry of Ukraine for Education and Science (Grant no. 0111U001088).

References

[1] F. Weitzer, P. Rogl, J. Phase Equilibria 15 (1994) 636.
[2] F. Weitzer, P. Rogl, J. Phase Equilibria 14 (1993) 676.
[3] B. Malaman, G. Venturini, B. Roques, Mater. Res. Bull. 23 (1988) 1629.
[4] T. Mazet, R. Welter, B. Malaman, J. Magn. Magn. Mater. 204 (1999) 11.
[5] B. Malaman, G. Venturini, B. Roques, Mater. Res. Bull. 24 (1989) 231.
[6] X.-W. Lei, G.-H. Zhong, M.-J. Li, G.-J. Mao, J. Solid State Chem. 181 (2008) 2448.
[7] X.-W. Lei, C.-L. Hu, G.-J. Mao, J. Solid State Chem. 183 (2010) 2032.
[8] L.G. Akselrud, Yu.N. Grin, P.Yu. Zavalii, V.K. Pecharsky, V.S. Fundamenskii, Collect. Abstr. 12th Eur. Crystallogr. Meeting, vol. 3, Nauka, Moscow, 1989, p. 155.
[9] W. Kraus, G. Nolze, PowderCell for Windows (Version 2.4), Federal Institute for Materials Research and Testing, Berlin, March 2000.
[10] J. Rodriguez-Carvajal, FULLPROF: A Program for Rietveld Refinement and Pattern Matching Analysis, Version 3.5d, Laboratoire Léon Brillouin (CEA–CNRS), Saclay, France, 1998.
[11] G.M. Sheldrick, SHELXS97 and SHELXL97, University of Göttingen, Germany, 1997.
[12] T.B. Massalski, Binary Alloy Phase Diagr., ASM, Metals Park, OH, 1990.
[13] P. Villars, L.D. Calvert, Pearson's Handbook of Crystallographic Data for Intermetallic Phases, ASM, Metals Park, OH, 1991.
[14] G. Venturini, M. Francois, B. Malaman, B. Roques, J. Less-Common Met. 160 (1990) 215–228.
[15] M. Francois, G. Venturini, B. Malaman, B. Roques, J. Less-Common Met. 160 (1990) 197–213.
[16] L. Romaka, V. Pavlyuk, V. Romaka, B. Marciniak, Visnuk Lviv. Univ. Ser. Khim. 51 (2010) 31.
[17] C. Lefevre, A. Verniere, G. Venturini, B. Malaman, J. Alloys Compd. 361 (2003) 40.

[18] M.L. Fornasini, F. Merlo, G.B. Bonino, Atti Accad. Naz. Lincei, CI Sci. Fis. Mater. Nat. 50 (1976) 186 (in Italian).
[19] P. Salamakha, O. Sologub, G. Bocelli, S. Otani, T. Takabatake, J. Alloys Compd. 314 (2001) 177.
[20] F. Weitzer, A. Leithe-Jasper, K. Hiebl, Q. Qi, P. Rogl, J.M.D. Coey, J. Appl. Phys. 73 (1993) 8447.
[21] B.C. Idrissi, G. Venturini, B. Malaman, Mater. Res. Bull. 26 (1991) 1331.
[22] R.R. Olenitch, L.G. Akselrud, Ya.P. Yarmolyuk, Dopov. Akad. Nauk Ukr. RSR Ser. 2A (1981) 84.
[23] B. Malaman, G. Venturini, B. Chafik, E. El Idrissi, Ressouche, J. Alloys Compd. 252 (1997) 41.